Smart Structures and Systems, *Vol. 28, No. 0 (2021) 000-000*
https://doi.org/10.12989/sss.2021.28.0.000

Predicting wind-induced structural response with LSTM in transmission tower-line system

Jiayue Xue [a] and Ge Ou*

Department of Civil and Environmental Engineering, University of Utah, 110 Central Campus Dr., Ste. 2000, Salt Lake City, UT, United States

(*Received November 26, 2020, Revised March 10, 2021, Accepted March 16, 2021*)

Abstract. Wind-induced dynamic response of the nonlinear structure is critical for the structural safety and reliability. The traditional approaches for this response including observation or simulation focus on the structural health monitoring, the experiment, or finite element model development. However, all these approaches require high cost or computational investment. This paper proposes to predict the wind-induced dynamic response of the nonlinear structure with a novel deep learning approach, LSTM, and applies this in a structural lifeline system, the transmission tower-line system. By constructing the optimized LSTM architectures, the proposed method applies to both the linear structure, the single transmission tower and the nonlinear structure, the transmission tower-line system, with promising results for the dynamic and extreme response prediction. It can conclude that the layers and the hidden units have a strong impact on the LSTM prediction performance, and with proper training data set, the computational time can significantly decrease. A comparison surrogate model developed by CNN is also utilized to demonstrate the robustness of the LSTM-based surrogate model with limited data scale.

Keywords: dynamic response; nonlinear structure; LSTM; RNN; wind engineering

1. Introduction

The structural dynamic response induced by severe windstorms is one of the main reasons that cause structural damage or collapse (Repetto and Solari 2010). In 2018, Hurricane Michael, attacked Mexico Beach and Florida, with 1584 out of 1692 buildings damaged in Mexico Beach and more than 1000 buildings damaged or destroyed in Florida, Alabama and Georgia (NOAA 2018). In 2019, Hurricane Dorian made landfall and caused numerous powerlines damaged, which impacted more than 190,000 people in coastal South Carolina (NOAA 2019). Due to the temporal and spatial stochastic characteristics of the wind loads, wind-induced vibration is a vital index to evaluate the structural condition like the damage or fail of the high-rise buildings, bridges, and the transmission infrastructures.

The traditional approaches to obtain the wind-induced vibration includes the structural health monitoring (SHM), field or laboratory experiment, and the finite element model development. Structural health monitoring is a favorable method to detect the structural response during its service period by implementing monitors (Ghoshal *et al*. 2000, Ni *et al*. 2007, Jang *et al*. 2010, Park *et al*. 2016). Wong *et al*. (2000) employed SHM by installing the monitors at the top and the deck level of the bridges to obtain the structural wind response of three cable-supported bridges in Tsing Ma Control Area. The wind rose diagrams, deck responses, wind turbulence intensities and spectra are all obtained in this process. Park *et al*. (2008) utilized a linear mass shaker and an active tuned mass damper to simulate the building's wind induced response and the results demonstrated that this excitation system can reproduce the structural response of each structural floor. Park and Oh (2018) implemented this on the tallest building in Korea, Lotte World Tower and concluded that the difference of damping was induced by wind excitation. Field or laboratory experiment is another satisfying approach to observe the structural vibration induced by wind loads (Levitan *et al*. 1991, Tamura *et al*. 2002, Zhu *et al*. 2012). The researchers conducted the field test to have the full-scale measurement of the continuous and simultaneous wind-induced structural response (Chen *et al*. 2001a, b, Molinari *et al*. 2011); and to compare the full-scale field test with the wind tunnel measurement (Zhang and Li 2018, Hua *et al*. 2019). The finite element model is also a popular method to simulate the structural dynamic response during wind loads (Geurts *et al*. 1998, Hamada *et al*. 2010). Hong *et al*. (2011) developed a finite element model of an existing suspension bridge and updated the model to predict its wind-excited dynamic response with promising accuracy. Fu *et al*. (2016) generated the finite element model of the transmission tower and predicted its dynamic response during the wind and rain load. Different wind attack angles and wind spectrums are considered in this process and the reliability of the transmission tower are obtained as well. He *et al*. (2018) employed a three-dimensional finite element model of the low-rise wood-frame building to observe the dynamic response during the wind loading. They concluded that the response generated from the finite element model demonstrates the reasonable agreement with the experimental results. However, the

*Corresponding author, Assistant Professor,
E-mail: ge.ou@utah.edu
[a] Ph.D. Candidate, E-mail: jiayue.xue@utah.edu

ISSN: 1738-1584 (Print), 1738-1991 (Online)

SHM and the field or laboratory experiment is usually limited by the site condition and the expense. The finite element model is usually computationally expensive, especially for the reliability or regional analysis considering a large set of uncertainties.

With the development of the machine learning methods, employing the surrogate model to predict the structural dynamic response has stimulated researchers to explore. The existing literature focuses on obtaining the extreme structural performance and the time history response during the wind loads (Le and Caracoglia 2020, Fang *et al*. 2020, Micheli *et al*. 2020). For the extreme structural performance, Oh *et al*. (2019) derived the surrogate model of a tall building during the wind loads to estimate the maximum and minimum strains with high accuracy compared with the experimental data. The results prove that this machine learning-based model can capture the uncertainties that are not available for the finite element model, and it can avoid big data collection. Hu *et al*. (2020) extended this work and developed surrogate models based on four different machine learning methods. They summarized that the generative adversarial networks (GANs) have the best performance to predict the pressure coefficients and predict them based on 30% dataset, which largely saves the cost of the wind tunnel tests. The research about developing the surrogate model of structural time history analysis during the wind loads is limited. Xue *et al*. (2020) utilized Convolutional Neural Network (CNN) to predict the dynamic response of the transmission tower during the extreme wind. The results illustrate promising results that this surrogate model can estimate the time history response, the extreme displacement, and the reliability of the transmission tower's performance. Moreover, the uncertainties of the wind profiles and spectrums are captured by this CNN based surrogate model.

However, some limitations exist in the previous research: 1) The surrogate model for the time history response of the structure during the wind is limited. The entire time history of the structure provides integrated information of the structural performance, which helps further analysis or reinforcement. 2) The current research about the surrogate model development applies to the linear structure, the transmission tower, while to the authors' best knowledge, research involves the large nonlinearity of the structure during the wind loads is at the initial stage. Large nonlinearity performance of the structure is challenging for the finite element model development, computation, and the surrogate model development. 3) The dataset generation for the surrogate model development is a tedious task with the high computational requirement. The surrogate model developed by CNN (Xue *et al*. 2020) required generating 100 samples with 600 seconds time history response of the transmission tower. However, when it comes to the nonlinearity analysis, this data amount could be a burden.

To fill this gap, this paper proposes to employ Long Short Term Memory (LSTM), an improved recurrent neural network (RNN) to develop the surrogate model of the transmission tower/tower-line system during the wind loads to capture the dynamic linear and nonlinear response. The initial concept of RNN was proposed by Hopfield (1982) to build a neural network with a function of content memorization. An improvement was made by Jordan (1986) to integrate it with backpropagation and utilize logistic as the activation function. Later, another improvement was proposed by Elman (1990) who designed a full connected RNN. However, RNN cannot predict long sequence that had long time dependence due to the problems of gradient vanishing and gradient explosion. To solve this issue, long short-term memory (LSTM) networks were reported (Hochreiter and Schmidhuber 1997) by introducing a cell consisting of a forget gate, input gate, and output gate. After that, LSTM has been used as a deep learning method to predict time sequences in various areas. To date, the LSTM is mainly utilized on the seismic response prediction of the structures. Zhang *et al*. (2019) employed LSTM to predict the nonlinear structural response during the seismic loads. The results demonstrate that this is a robust approach for the nonlinear structural response during the large seismic intensities. However, the application proposed is limited to a single input system, the feasibility and performance of LSTM with multiple inputs still require investigation.

Dynamic wind loads are composed by the mean and fluctuating wind when conducting the structural dynamic analysis. The mean wind is generated based on the theoretical formulas such as the power law or logarithm law (ASCE 1999). The fluctuating wind is a stochastic process generated from a power spectrum and the spatial correlation is realized by a cross-spectral density spectrum (Davenport 1961). Hence, a strong temporal and spatial correlation of the wind loads is presented for the dynamic analysis, which increases the complexity to develop the LSTM-based surrogate model. Such temporal and spatial correlation will

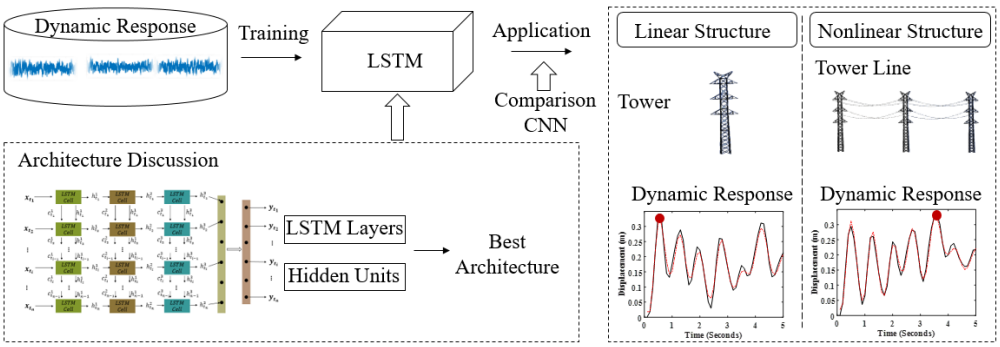

Fig. 1 The flowchart of an LSTM-based surrogate model development

be amplified to large scale spatial distributed structures such as bridges and transmission towers-line system. To investigate the performance of LSTM model with complex loading and structural setup, this paper utilizes the transmission tower-line system as a target structure, the flowchart is demonstrated in Fig. 1.

By constructing the appropriate architecture of LSTM from the generated training data, the dynamic response of the linear and nonlinear structure during the wind loads are obtained. In the following sections, the architecture of LSTM, the LSTM cell, and its application to the infrastructure are presented. The numerical model of the transmission tower/tower-line generation during the wind loads for the dataset of the surrogate model development are introduced in Section 3. A set of tests to optimize the LSTM architecture, including its layers, hidden units, and the training dataset choices, are conducted in Section 4. Section 5 applies the constructed LSTM architecture on the single transmission tower, a linear structure and the transmission tower-line system, a nonlinear structure to test its performance. A surrogate model developed by CNN is chosen as an index to compare the performance with the surrogate model developed by LSTM. In Section 6, the architecture and performance of LSTM are summarized, and the future work is discussed as well.

2. Methodology

As discussed in the previous section, LSTM is an advanced approach to obtain the nonlinear structural dynamic response during the seismic loads while its application in the wind engineering is not fully explored. This paper will employ LSTM to develop the surrogate model of the nonlinear structural response during the intensive wind by constructing the architecture of LSTM, discussing its cell and applying it into the surrogate model development of the civil infrastructure.

2.1 Architecture of LSTM

In general, the dynamic response of wind-induced infrastructure is temporal dependent, i.e., the structural response at time step A depends on a series of inducements in the previous steps. Thus, the selected surrogate model for sequence prediction should memorize the useful message in the previous time steps. As mentioned above, recurrent neural network (RNN) is a machine learning method to capture information in a sequence and has been widely used in a neural language process (Mirowski and Vlachos 2015, Yin *et al*. 2017, Morchid 2018) while it can only memorize a few steps and may fail in the case of long term dependence (Zhang *et al*. 2019). To overcome this drawback, long short-term memory (LSTM) elaborately merges short memory and long memory by introducing gate control units, which will be discussed in the following sections. Hence, this paper adopts LSTM to predict the wind-induced dynamic response.

Fig. 2 illustrates the overall architecture of deep LSTM, which involves the input layer, $lstm$ layers, fully connected layers, and the output layer. The input data is a temporal sequence $\{\boldsymbol{X}_{t_1}, \boldsymbol{X}_{t_2}, \dots, \boldsymbol{X}_{t_n}\}$, where t_n is the time length of the sequence, and $\boldsymbol{X}_{t_i}$ denotes the wind speeds of the study points on the structure at time t_i. The $\boldsymbol{X}_{t_i}$ is calculated as $\{v_{p_1}, v_{p_2}, \dots v_{p_i}, \dots\}_{t_i}^{T}$, in which v_{p_i} is the wind speed at point p_i. The processed results of the cell are $c_{t_i}^1$ and $h_{t_i}^1$, where $c_{t_i}^1$ is the cell state and $h_{t_i}^1$ is the hidden state. These two outputs and $\boldsymbol{X}_{t_{i+1}}$ are then processed by the next cell in the same layer. In this process, the cell state $c_{t_i}^1$ is used to deliver information at time step t_i to the cells at successive time steps, and the hidden state $h_{t_i}^1$ is the input of a cell in the next $lstm$ layer. The detailed operation of $lstm$ cell will be discussed in Section 2.2. It should be noted that the hidden state is a vector combined with several units (called hidden units) rather than a single unit. It makes the remembered information more representative. After calculating the first $lstm$ layer, the subsequent $lstm$ layers repeat the same processing. After that, it is connected by the fully connected (FC) layers. To reduce overfitting, half units in the FC layer are randomly selected and dropped. Finally, a regression output layer is created to generate a dynamic response.

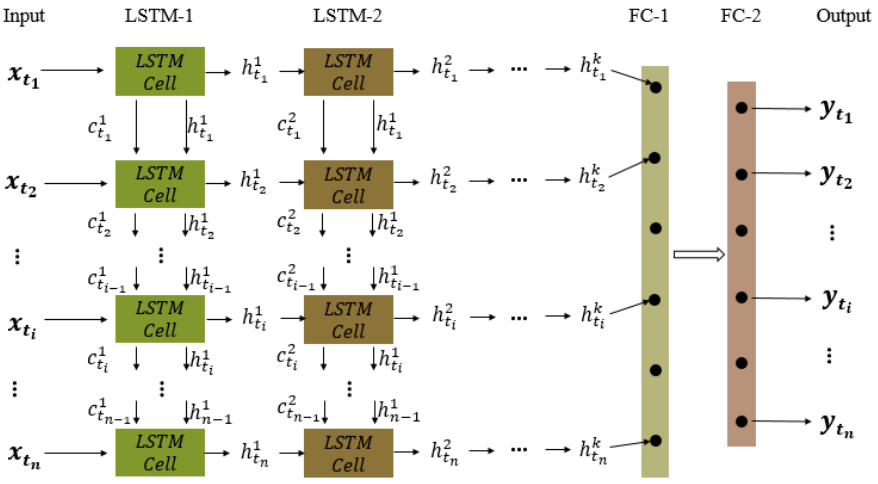

Fig. 2 Architecture of long short-term memory

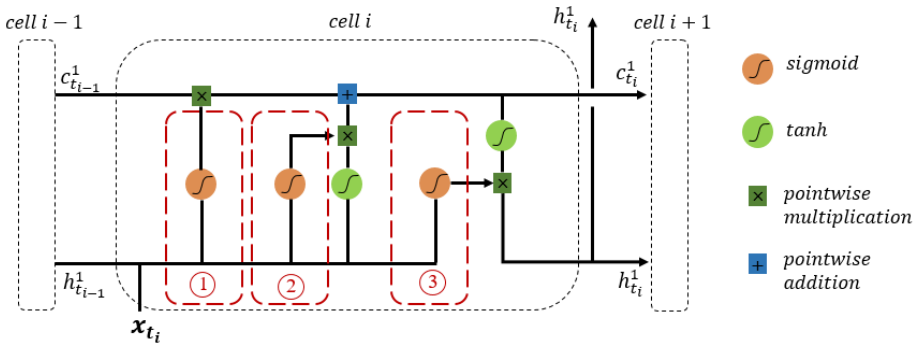

Fig. 3 Detailed operation of LSTM cell

2.2 Core component of memorization- the LSTM cell

The most remarkable feature of LSTM is that it deploys gates in a cell to merge short memory (information in a short time length) and long memory (information in a long time length). These gates calculate the importance of the information and decide to keep or forget the information. The operation details of LSTM cell are shown in Fig. 3, which involves three gates: forget gate (marked as ①), input gate (marked as ②), and output gate (marked as ③). In this figure, there is an unbroken vertical arrow that transforms information from the previous time steps to the latter time steps through the cell state $c_{t_i}^1$. There are two updates for cell state: one is generated by the forget gate, and another is the input gate.

First of all, the forget gate is designed to determine whether the new input in the current step should be dropped or not. To accomplish this goal, an activation function is introduced to produce an output value between 0~1 based on the input. The input is memorized if the output is close to 1; otherwise, the input is dropped if the output is close to 0. Herein, this research selects sigmoid since it is one of the simplest activation functions that can efficiently generate output within 0~1. It should be noted that other activation functions (e.g., ReLu) cannot constrain the output in a range, which is not satisfied with the purpose of designing gates in the LSTM. It is the same reason to utilize sigmoid function in the rest two gates. Therefore, a sigmoid function is developed as Eq. (1), where w_f and b_f are the weight and bias respectively, to process the hidden state $h_{t_{i-1}}^1$ in the previous step and the input $\boldsymbol{X}_{t_i}$ in the current step. The pointwise multiplication between the result $\boldsymbol{f}_{t_i}$ of forget gate and the cell state $c_{t_{i-1}}^1$ is then calculated to obtain an updated cell state. If $\boldsymbol{f}_{t_i}$ is close to 0, the cell state from previous time steps will be dropped; If $\boldsymbol{f}_{t_i}$ is close to 1, the information will be memorized and transformed to the following time steps. In this way, the information can be memorized in a long-time step, which is the improvement from classical RNN.

$$\boldsymbol{f}_{t_i} = \sigma(w_f \cdot [h_{t_{i-1}}^1, \boldsymbol{X}_{t_i}] + b_f) \tag{1}$$

The input gate is to deliver new information into the cell state, including a sigmoid operation and a $tanh$ operation. As it generates an output between -1~1 with a center of zero, $tanh$ operation is selected. The gradient around zero is large enough to increase the model convergence. The $tanh$ operation does not determine whether the input should be memorized or not, but only amplifies or reproduces the input. Similar to the forget gate, the hidden state $h_{t_{i-1}}^1$ and the input $\boldsymbol{X}_{t_i}$ are processed by a sigmoid function to get an importance factor $\boldsymbol{I}_{t_i}$. Meanwhile, $h_{t_{i-1}}^1$ and $\boldsymbol{X}_{t_i}$ are passed to a $tanh$ function to generate candidate values $\widetilde{\boldsymbol{C}}_{t_i}$ for updating the state cell. The sigmoid and $tanh$ operations are expressed in Eqs. (2)-(3), where $w_{I/C}$ and $b_{I/C}$ are the weight and bias, respectively. At last, the importance factor $\boldsymbol{I}_{t_i}$ and the candidate values $\widetilde{\boldsymbol{C}}_{t_i}$ are multiplied together, and the result is added to the cell state. By now, the cell state is updated as $c_{t_i}^1$ and ready to transform to the $lstm$ cell in the next time step. If $\boldsymbol{I}_{t_i}$ reach 0, the $\widetilde{\boldsymbol{C}}_{t_i}$ plays a vital role in the updated cell state and vice versa.

$$\boldsymbol{I}_{t_i} = \sigma(w_I \cdot [h_{t_{i-1}}^1, \boldsymbol{X}_{t_i}] + b_I) \tag{2}$$

$$\widetilde{\boldsymbol{C}}_{t_i} = tanh(w_C \cdot [h_{t_{i-1}}^1, \boldsymbol{X}_{t_i}] + b_C) \tag{3}$$

The final output gate is to generate the new hidden state. There are also two steps in this gate: sigmoid operation and $tanh$ operation. The sigmoid operation is for the hidden state $h_{t_{i-1}}^1$ and the input $\boldsymbol{X}_{t_i}$, and the function is shown in Eq. (4), where w_o and b_o are the weight and bias, respectively. The $tanh$ operation is for the updated cell state $c_{t_i}^1$ and expressed in Eq. (5). The sigmoid and $tanh$ outputs are multiplied, and the result is set as the updated hidden state $h_{t_i}^1$. Besides, the new hidden state $h_{t_i}^1$ is duplicated and passed to the $lstm$ cell in next $lstm$ layer (Fig. 2).

$$\boldsymbol{o}_{t_i} = \sigma(w_o \cdot [h_{t_{i-1}}^1, \boldsymbol{X}_{t_i}] + b_o) \tag{4}$$

$$\boldsymbol{tc}_{t_i} = tanh(c_{t_i}^1) \tag{5}$$

2.3 Application in civil infrastructure response prediction under dynamic inputs

There are two scenarios of LSTM applications to structure response prediction during dynamic inputs: 1) predicting the complete sequence of the dynamic response of the structure, and 2) predicting the extreme response of

the structure. The former scenario generates a surrogate model that can replay and predict the dynamic response under the wind inducement. The latter scenario is to obtain the extreme state that may cause the failure of the structure under the strong wind.

(1) Complete Sequence Prediction. The output is the complete sequence of dynamic response $\{\boldsymbol{Y}_{t_1}, \boldsymbol{Y}_{t_2}, \dots \boldsymbol{Y}_{t_2}, \dots, \boldsymbol{Y}_{t_n}\}$, where t_n is the time length of the sequence, and $\boldsymbol{Y}_{t_i}$ is a response vector consisted of the displacements of all interested points at time t_i.

(2) Extreme Response Prediction. The output is the extreme value in the complete dynamic response: $\boldsymbol{Y}_{max} = max\{\boldsymbol{Y}_{t_1}, \boldsymbol{Y}_{t_2}, \dots \boldsymbol{Y}_{t_2}, \dots, \boldsymbol{Y}_{t_n}\}$. Thus, the right layer in Fig. 2 will be redesigned as $\boldsymbol{Y}_{max}$. Unlike the complete sequence prediction, this scenario only predicts one value, the most critical index for structural failure. In other words, it is efficient to predict the desired value with less computation cost.

To evaluate the performance of LSTM on structure, this paper introduces a widely used RMSE (root mean square error) as the criterion. The expression of RMSE is presented in Eq. (6), where $\widetilde{y_{ti}}$ is the predicted value, and y_{ti} is the target value.

$$RMSE = \sqrt{\frac{1}{n}\sum_{i=1}^{n}(\widetilde{y_{ti}} - y_{ti})^2} \tag{6}$$

3. Numerical modeling of the transmission tower/tower-line structure system during wind loadings

In this paper, the proposed LSTM architecture is implied to predict the dynamic response of the transmission tower/tower-line during the wind load. There are two reasons to choose the transmission tower/tower-line system as the representative structure. 1) As a vital lifeline structure, the transmission tower/tower-line system is vulnerable to the extensive wind because of its complex vibration. The geometric nonlinearity of this transmission tower/tower-line system is one of the critical factors that leads to structural damage. 2) In three-dimensional space, the transmission tower/tower-line system is configured by thousands of nodes. Wind loads are complex on this structure with time and spatial correlation. Therefore, the transmission tower/tower-line system is representative to generate the data set for the LSTM architecture development.

3.1 Development finite element model of transmission tower-line system

To generate the dataset for training and testing purpose, the finite element model of the transmission tower/tower-line system is developed by ANSYS/LS-DYNA as Fig. 4

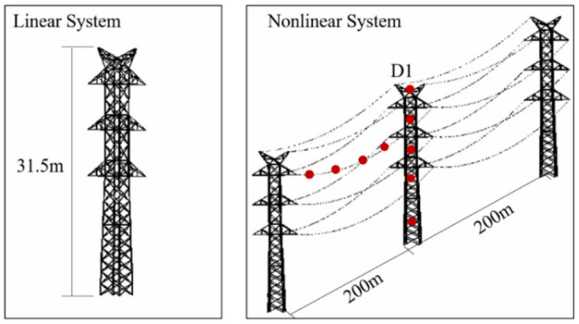

Fig. 4 Finite Element Model of Transmission Tower/ Tower-Line System

demonstrates. This initial transmission tower is from Tort *et al*. (2017) and redesigned (Xue *et al*. 2020). This is a suspension tower with 31.5 m height and 200 m span between two transmission towers. The cross sections of the transmission towers are L-shaped. The sag of both ground line and conductor is 2.9 m and 3.7 m. There are thousands of nodes of the transmission tower-line system, which makes it impossible to add the wind load on each node. This paper chooses 79 representative points with 5 and 4 points on each transmission tower and line, respectively. The dynamic wind loadings are added on these representative points to obtain the linear and nonlinear response of the transmission tower/tower line system. Wind load generation is presented in Section 3.2. The top displacement D1 of the middle transmission tower is considered as the index of the dynamic response of the transmission tower/tower-line system.

3.2 Wind load input and structural dynamic response

The complexity of the wind load is due to its temporal and spatial correlation. The stochastic wind $V(t)$ is simulated by the mean wind $\bar{V}$ and the fluctuating wind V_j as shown in Eq. (7). According to ASCE 7-98 (ASCE 1999), the mean wind profile changes along with the height by a power law as Eq. (8).

$$V(t) = \bar{V} + V_j \tag{7}$$

$$\frac{\bar{V}}{\bar{V}_{10}} = \left(\frac{z}{z_{10}}\right)^{\alpha} \tag{8}$$

where $\bar{V}_{10}$ is usually taken as the reference wind at 10 m height; z is the height of the mean wind speed; z_{10} is the reference height; α is determined by the ground roughness.

The temporal and spatial correlation of the fluctuating wind is realized by a Gaussian stationary random process and the Davenport spectrum (Davenport 1961). By the Cholesky decomposition, the fluctuating wind $v_j(y_j, z_j, t)$ is obtained as Eqs. (9)-(10).

$$v_j(y_j, z_j, t) = \sqrt{2(\Delta\omega)}\sum_{m=1}^{j}\sum_{l=1}^{N}\left|H_{jm}(\omega_{ml})\right| cos\left(\omega_{ml}t - \theta_{jm}(\omega_{ml}) + \varphi_{ml}\right) \tag{9}$$

$$j = 1,2,\cdots, nt$$

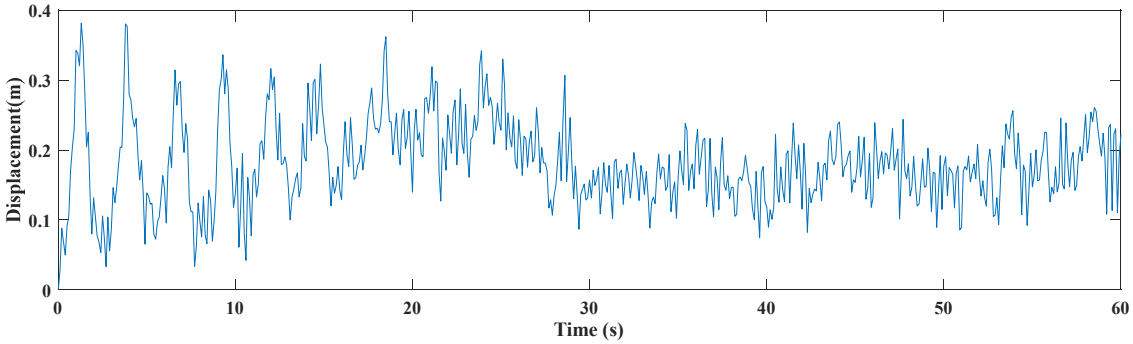

Fig. 5 Dynamic response of the middle transmission tower-line system

$$\omega_l = (l-1)\Delta\omega + \frac{m}{N}\Delta\omega, \qquad l = 1,2,\cdots,N \tag{10}$$

where H(ω) is from the Cholesky decomposition; $\Delta\omega$ is the frequency increment.

As the dynamic wind is simulated, the wind load on each node of the transmission tower/tower-line system can be calculated as Eq. (11).

$$\mathrm{F} = 0.5\rho V(t)^2 C_f \mathrm{A}_m \tag{11}$$

where ρ, C_f and A_m are the air density, drag coefficient nd the projected area respectively.

As the top displacement of the transmission tower is usually chosen as the failure or damage index, here is the dynamic response after adding the dynamic wind loads on the top of the middle of the transmission tower-line system as shown in Fig. 5.

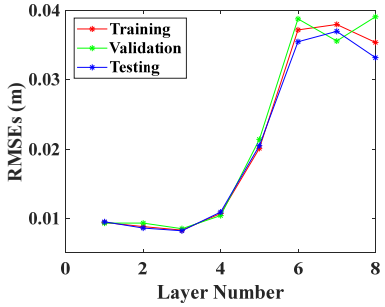

Fig. 6 RMSEs of different layer numbers

4. LSTM architecture optimization

As mentioned in Section 3, the layer numbers and the hidden units of the LSTM architecture, are the two parameters that may affect the prediction performance of the LSTM network. According to the existing studies (Cabada *et al*. 2020, Reimers and Gurevych 2017, Zhou and Song 2020), different architectures of deep learning methods may significantly differ in the computational time and prediction accuracies. Besides, the scale of the training dataset is another fundamental factor that may cause the difficulty due to the processing time for different data size and the generalization ability for different data coverage. Hence, this section will discuss the influence of LSTM architecture (layer numbers and hidden units) and training dataset on the LSTM performance. The prediction accuracy (the aforementioned RMSE) and the computational time are selected to evaluate the performance. Simultaneously, to save the computational time for both the data generation and training, the dynamic response of the linear structure, the single transmission tower during the wind load is employed. The constructed architecture will be tested on the nonlinear structure, the transmission tower-line system in ection 5. The dynamic winds are added on the nodes of the transmission tower as Fig. 4 demonstrates. The top displacement, D1 as shown in Fig. 4, is chosen as the index for the dynamic response of the transmission tower. As stated above, the input of LSTM is the wind loads that applied to the representative points in the transmission tower/tower-line system, and the output is the top displacement of the transmission tower. This FEM model is utilized to generate the training and testing dataset. The training and testing dataset involved in this paper are

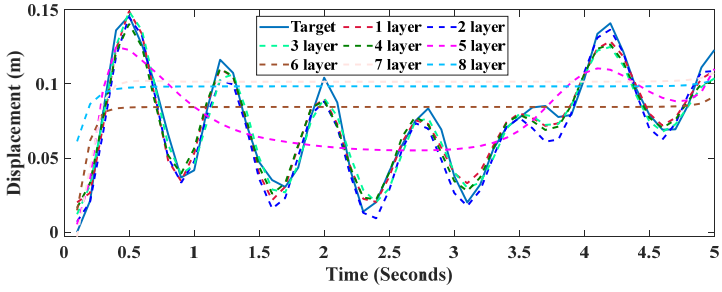

Fig. 7 Prediction performance under different LSTM layer number

Table 1 Computational time under different layer numbers

Layers	1	2	3	4	5	6	7	8
Training (s)	17.22	29.63	40.64	53.15	67.34	79.37	91.15	110.81
Testing (s)	0.10	0.11	0.10	0.13	0.14	0.13	0.14	0.17

implemented on a computer with the specifications of Intel i7-8920H CPU, Navidia GTX 9470, and 16 GB RAM.

4.1 Influence of LSTM architecture on the prediction performance

In this section, the influence of LSTM architecture on the prediction accuracy is discussed. 400 samples of the dynamic response of the transmission tower induced by wind speed of 35 m/s are simulated. 5 seconds time length with a sampling frequency of 10 Hz are chosen as in the previous literature (Xue *et al*. 2020), this time length with proper time convention has highest accuracy with appropriate computational time. Among these samples, 240 samples (60%) are used as training dataset, 80 samples (20%) are used as validation dataset, and 80 samples (20%) are used as testing dataset.

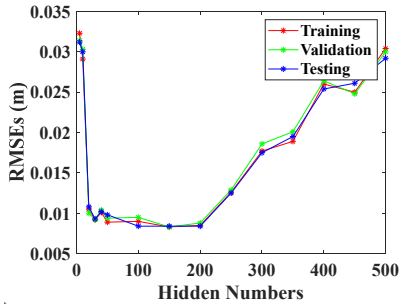

Fig. 8 RMSEs under different hidden units

4.1.1 Optimization of LSTM layers

To evaluate the layer numbers, this research designs eight different cases from 1 layer to 8 layers. The number of hidden units for each layer is 200. The RMSEs of these eight cases are shown in Fig. 6, which contains the performance on training, validation, and testing datasets. It clearly illustrates when there are 3 layers, the RMSE is smallest. In addition, the prediction accuracy decreases with the increase of the layer numbers. Fig. 7 illustrates the dynamic responses predicted by different cases, which shows that the first three cases (1 layer, 2 layers, and 3 layers) have a better performance than the other cases. In addition, the computational times of both training and testing datasets significantly increase along the increase of layer numbers (Table 1). In summary, the LSTM layer numbers influence the prediction accuracy and computational time simultaneously. Thus, this research selects 3 layers as the optimized LSTM network, which has the lowest RMSE and acceptable computational time.

4.1.2 Optimization of LSTM hidden units

The hidden units in LSTM denote the parameter numbers in the hidden state (Fig. 2) and store the short memory. To evaluate the impact of hidden units on the LSTM performance, this research designs the cases of different unit numbers from 5, 10, 20, 30, 40, and 50 to 800 with an increase of 50. The optimized 3 layers are used to discuss the hidden unit optimization. The RMSE and computational time under different hidden unit numbers are shown in Fig. 8 and Table 2, respectively. It's found that:

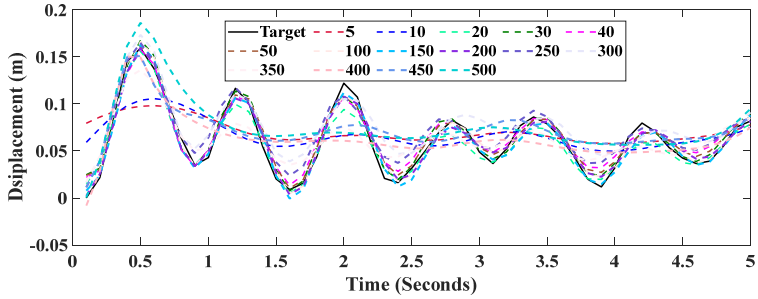

Fig. 9 Prediction of top displacement of transmission tower under wind loading with different hidden units

Table 2 Computational time under different hidden units

Hidden units	5	10	20	30	40	50	100	150
Training (s)	33.63	31.81	32.87	27.93	31.83	28.50	30.11	32.09
Testing (s)	0.08	0.10	0.11	0.11	0.10	0.11	0.10	0.10
Hidden Units	200	250	300	350	400	450	500	
Training (s)	41.73	42.46	47.81	60.38	61.68	74.77	79.06	
Testing (s)	0.11	0.11	0.12	0.13	0.12	0.12	0.12	

(1) when the hidden number varies from 50 to 200, RMSE fluctuates in a small range, while when the hidden numbers are out of the range, the RMSE increases significantly; and (2) the computational time also increases smoothly with the growing hidden units. In addition, the dynamic responses predicted by the LSTMs with different hidden unit are illustrated in Fig. 9, which is consistent with the previous two findings. The predicted responses with hidden units from 50 to 200 are close to the target response, while the predicted responses with hidden units out of the range are far away from the target response. It demonstrates the selection of hidden units should not be extremely small or large. Therefore, this research selects 200 as the hidden units in the remaining discussion.

4.2 Impact of training dataset on the prediction performance

The size of training dataset is a critical parameter that can affect the prediction accuracy and the computational time of LSTM. A large dataset typically can obtain a promising prediction accuracy due to the strong generalization while more computing resources are involved in processing data. In this section, 3 layers and 200 hidden units optimized in the previous sections, are selected as the LSTM architecture. To train the network, a series of samples of the dynamic response of transmission tower are simulated. Each sample has 50 data points with a time length of 5 seconds and a frequency of 10 Hz, and the inducement wind is 35 m/s. To make the performance of different cases comparable, 100 samples are selected as a consistent testing dataset. The training samples vary from 50 to 800, in which 70% are training dataset, and 30% are validation dataset.

The RMSEs for the LSTMs trained by different data points are shown in Fig. 10, which demonstrates that the when the number of training data points are smaller than 300 samples ×50 data points, the RMSE is worse and worse with the decrease with the training samples. The RMSE has small vibrations when the number of training data points is larger than 400 samples ×50 data points. Fig. 11 presents the dynamic responses predicted by the LSTMs with different data points. It is found that the responses with larger data points are much closer to the target response than small data points. The computational times under different training data points are summarized in Table 3, which shows an increase of computational time with the increase of data points. Combining the results in Fig. 10 and Table 3, we can conclude that there is a trade-off between the RMSEs and the computational time when selecting the scale of training data points. The optimized number of training data points used in this research is 400 samples ×50 data points with a low RMSE and a reasonable computational time.

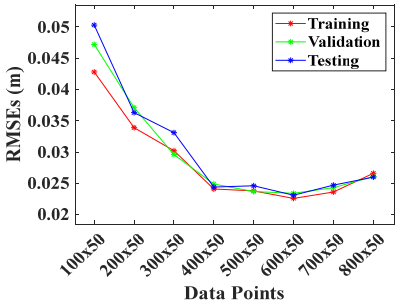

Fig. 10 RMSEs under different training samples

5. Results and discussion

This section evaluates the constructed LSTM architecture in Section 4 and compares its prediction performance with another deep learning method, Convolutional Neural Network (CNN), in the aspects of the full-time history response and the extreme value of the linear and nonlinear structure.

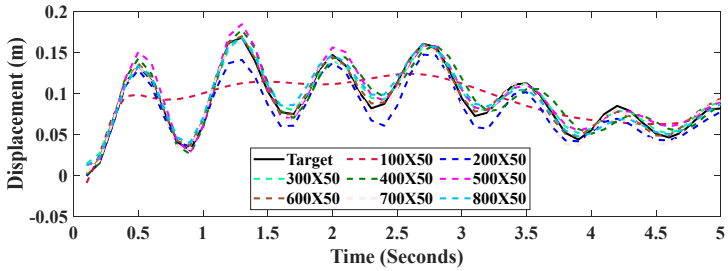

Fig. 11 Prediction performance under different training samples

Table 3 Computational time under different training samples

Data Points (sample* data point)	100×50	200×50	300×50	400×50	500×50	600×50	700×50	800×50
Training (s)	17.22	29.63	40.64	53.15	67.34	79.37	91.15	110.81
Testing (s)	0.10	0.11	0.10	0.13	0.14	0.13	0.14	0.17

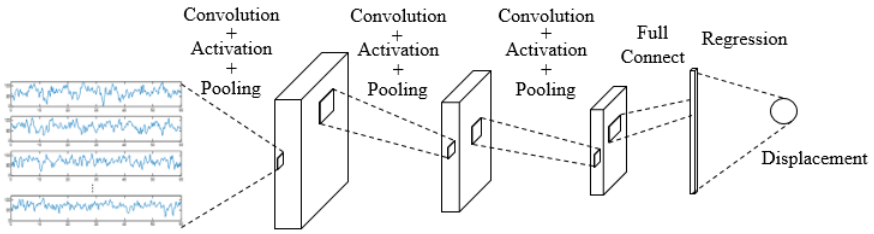

Fig. 12 CNN architecture

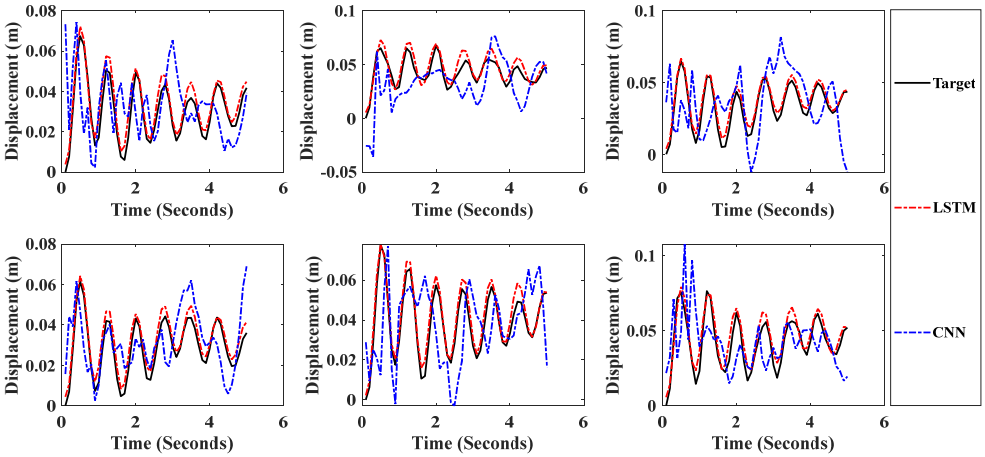

(a) Dynamic response prediction when wind speed is 20 m/s

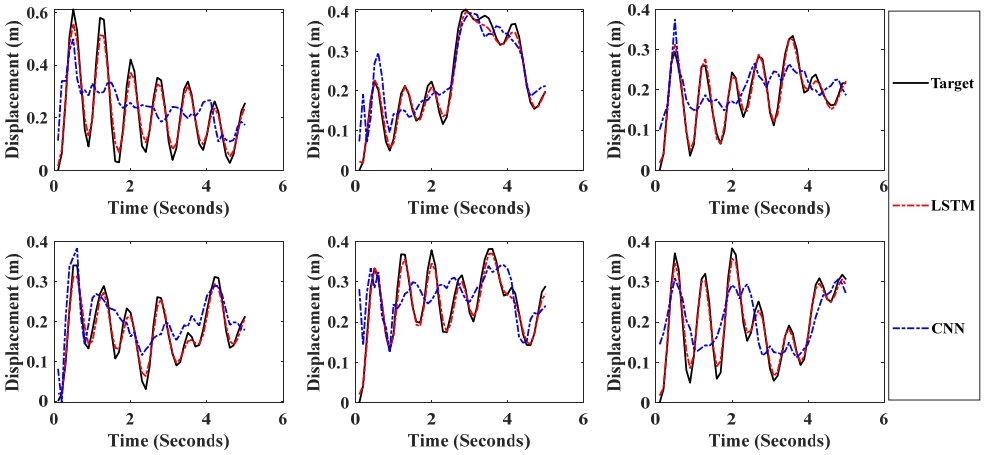

(b) Dynamic response prediction when wind speed is 60 m/s

Fig. 13 Dynamic response comparison of LSTM and CNN (Linear system)

5.1 Index to evaluate the prediction performance by LSTM architecture

The full-time history and the extreme performance of the structural dynamic response are two vital indexes to assess its damage or collapse. To show the superiority of the LSTM, CNN is developed as the comparison method. As demonstrated in our previous work (Xue *et al*. 2020), the wind loads on the structure are time and spatially correlated and can be formed as an image format, which is the typical input of CNN. Thus, CNN is an alternative method to predict the dynamic response of infrastructure. This research applies the CNN architecture (Fig. 12) in Xue *et al*. (2020) to this research as the comparison method.

As shown in Fig. 12, CNN contains three convolutional layers (consisted of convolution, activation, and pooling), a full connected layer, and a regression output layer. The kernel size and kernel number of the three convolutional layers are (7,8), (5,16), (3,32), respectively. A window with 10 data points is introduced to split the input into several small stacks, which are the inputs of the CNN. The window is moved point by point to split each sample, and the prediction is the last value of each window.

5.2 Dynamic response prediction performance of single transmission tower (linear system)

First, this research selects a single transmission tower,

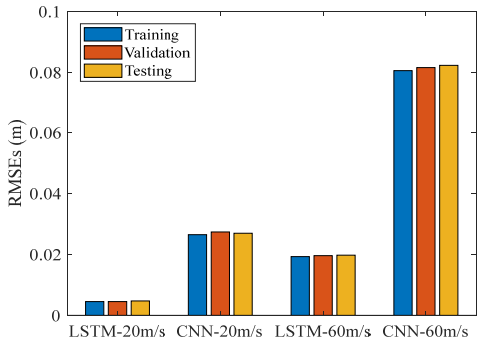

Fig. 14 RMSEs comparison of dynamic response predicted by LSTM and CNN (Linear system)

a linear system, as a study case to demonstrate the prediction capability of LSTM for dynamic response of the structure. The CNN architecture described above is utilized as the compared deep learning method. Two scenarios will be discussed here: (1) prediction of complete sequence, which can entirely provide the dynamic response of transmission tower; and (2) prediction of the maximum displacement, which indicates the extreme state of the tower under wind inducement.

The selected LSTM networks are three layers with 200 hidden units, the optimized architecture in the previous section. To obtain a promising performance, the data points used to train the network are 400 samples with 5 seconds wind time history and 10 Hz sampling frequency, in which 360 samples are training datasets, and 40 samples are validation samples. Another 100 samples are constantly designed to as testing dataset. To prove the robustness, the selected methods are tested on a low wind speed of 20 m/s, and an extensive wind speed of 60 m/s.

5.2.1 Prediction of complete dynamic response time series

After training the surrogate model based on the LSTM and the CNN, two networks are generated and validated with the testing dataset. Six samples for 20 m/s and 60 m/s are randomly selected and shown in Fig. 13, which demonstrates the superiority of LSTM. Although CNN can capture the rough trend of the dynamic response, the predictions of CNN are much far away from the targets on both 20 m/s and 60 m/s. Conversely, the LSTM can not only capture the trend of dynamic response but also predict more accurate values than that predicted by CNN.

The RMSEs of training, validation, testing datasets predicted by LSTM and CNN are shown in Fig. 14, which demonstrates for both 20 m/s or 60 m/s, the RMSEs of LSTM are entirely lower than CNN. This phenomenon indicates the superiority of LSTM for predicting the dynamic response. Even though the previous studies (Sun *et al*. 2017, Xue *et al*. 2020, and Wu and Jahanshahi 2019) have demonstrated the capability of the CNN to predict the dynamic response, the data points (time length × wind frequency) of each sample used in those studies are much longer than 50. Thus, when the data scale is limited for the further nonlinear structure analysis, CNN is not as suitable as LSTM to predict its dynamic response.

5.2.2 Extreme value prediction performance of linear single transmission tower

Another discussion is about the maximum displacement in the dynamic response of each sample as the maximum

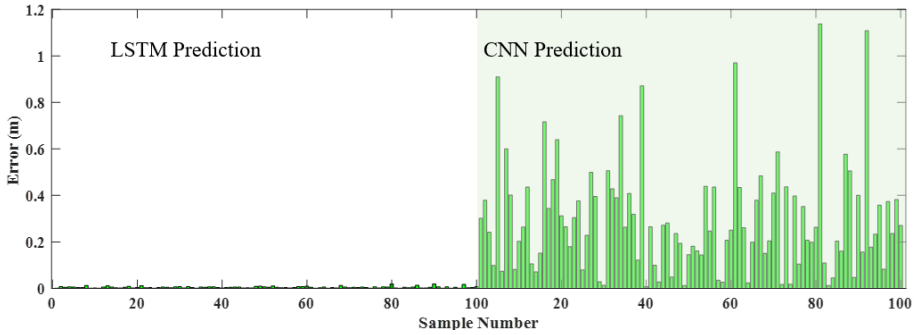

(a) Extreme value prediction when wind speed is 20 m/s

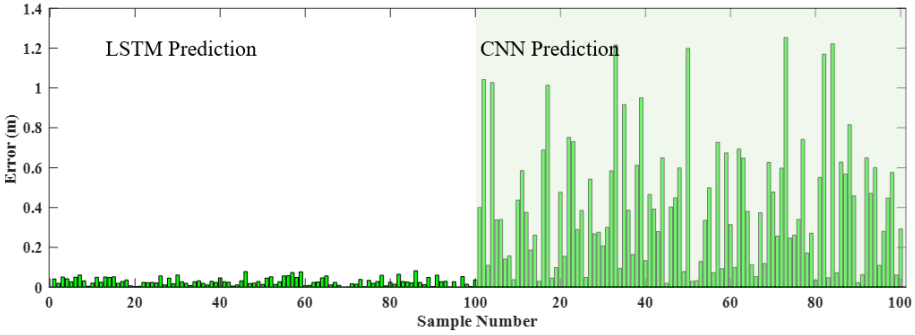

(b) Extreme value prediction when wind speed is 60 m/s

Fig. 15 Error comparison of maximum response (Linear system)

Table 4 RMSE and time comparison between different LSTM architectures

	RMSE_Training	RMSE_Validation	RMSE_Testing	Training time (s)	Test time (s)
LSTM_1L-5U	0.055	0.070	0.068	17.89	0.11
LSTM_1L-200U	0.045	0.065	0.061	22.82	0.12
LSTM_1L-500U	0.043	0.053	0.051	31.13	0.12
LSTM_3L-5U	0.042	0.045	0.043	34.13	0.11
LSTM_3L-200U	0.034	0.039	0.035	51.05	0.13
LSTM_3L-500U	0.041	0.047	0.045	107.37	0.12
LSTM_8L-5U	0.037	0.039	0.036	80.50	0.15
LSTM_8L-200U	0.069	0.069	0.069	133.94	0.15
LSTM_8L-500U	0.069	0.071	0.068	281.37	0.19

response is the indication of the extreme state of transmission tower under the inducement of strong wind. The maximum displacement leads to the severe state directly with a less computational cost.

The error between the target and the predicted maximum response for each sample in the testing dataset is plotted in Fig. 15, including the cases of 20 m/s and 60 m/s. As shown, the errors of LSTM prediction are less than 0.01 m for 20 m/s and less than 0.04 m for 60 m/s. This promising result proves the capability of LSTM to predict the maximum response of transmission tower. Similar to the prediction of the complete sequence, the errors of the LSTM prediction are always smaller than that of CNN. What's more, the error difference between the LSTM and CNN are more significant than the complete sequence prediction (Fig. 13), which represents that the LSTM is more suitable in predicting the maximum response than CNN.

5.3 Dynamic response prediction performance of transmission tower-line system (nonlinear system)

To expand the application of LSTM prediction from the linear structural system to the nonlinear system, a set of the transmission tower-line system are simulated for the dataset. Different LSTM architectures are constructed to test if the architecture developed by the linear structural system works for the nonlinear system. After that, the LSTM application in predicting the dynamic response and the extreme value of the transmission tower-line system and the comparison between the LSTM and the CNN is presented. There are a totally 500 samples, in which 320 samples are the training dataset, 80 samples are the validation dataset, and 100 samples are the testing dataset. Each sample has 50 data points with a time length of 5 seconds and a frequency of 10 Hz.

5.3.1 Optimal LSTM architecture validation

As discussed in Section 4, both the number of the LSTM layers and hidden units have a significant impact on the dynamic response prediction of the single transmission tower during the dynamic wind. To extend this linear structure to a nonlinear structural system, it is reasonable to test the developed LSTM architecture on the nonlinear structure. Therefore, nine different LSTM architectures with 1, 3, 8 layers, and 5, 200, 500 hidden units are developed. Besides, the wind speed used in this section is 60 m/s.

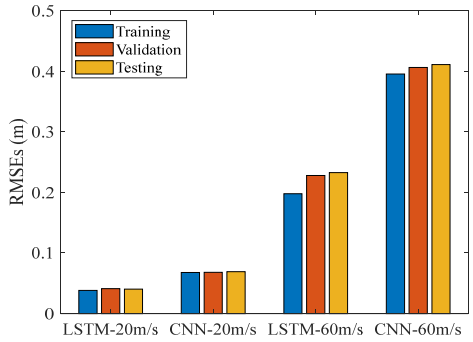

Fig. 16 RMSEs comparison of dynamic response predicted by LSTM and CNN (Nonlinear system)

The training, validation and testing RMSE and the training and testing time for the nonlinear structure, transmission tower-line system, are recorded and summarized as Table 4. It shows that the impact of different architectures on LSTM prediction agrees with the discussion in Section 4. The overall RMSEs are on the same scale as the results of linear structure (Fig. 14), and the best performance also happens in the case of 3 LSTM layers with 200 units. Herein, this research chooses 3 layers and 200 units as the architecture for the LSTM application to nonlinear structure.

5.3.2 Dynamic response prediction performance of nonlinear transmission tower-line system

The RMSEs of the training, validation, and testing datasets predicted by the LSTM and CNN are summarized in Fig. 16, involving 20 m/s and 60 m/s. It clearly demonstrates that the LSTM has lower RMSEs than CNN on both 20 m/s and 60 m/s. The dynamic response of the target, the LSTM, and CNN prediction are shown in Fig. 17. It's also found that the LSTM prediction can achieve promising RMSEs for both 20 m/s and 60 m/s. The dynamic responses predicted by the LSTM are close to the target and can successfully capture the trends. In addition, the results show that the predicted responses, for both LSTM and CNN based surrogate models, are much smoother than the target responses as the length of response

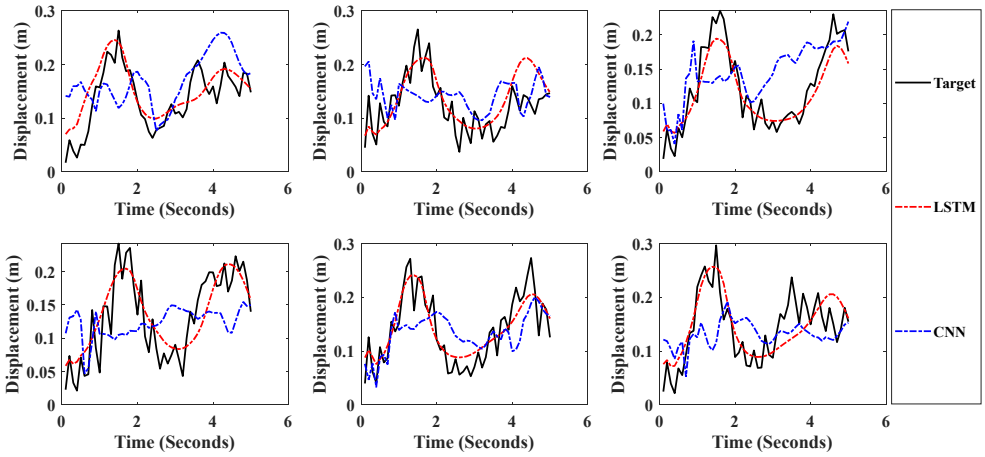

(a) Dynamic response prediction when wind speed is 20 m/s

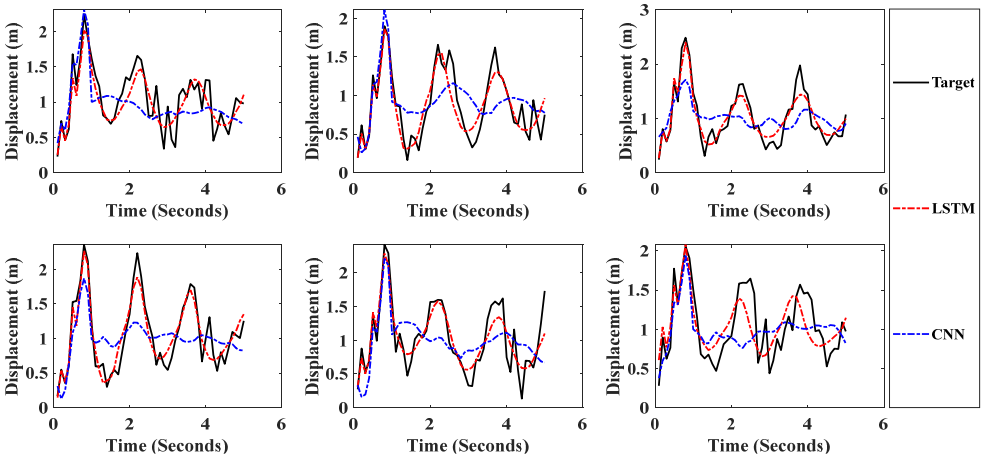

(b) Dynamic response prediction when wind speed is 60 m/s

Fig. 17 Dynamic responses of LSTM and CNN (Nonlinear system)

is only five seconds with fifty data points, which are limited in the prediction for the nonlinear structure. Currently, the proposed system can capture the outlines of the dynamic responses. Meanwhile, the prediction results for 20m/s appear larger deviations due to the small amplitudes of the dynamic responses for 20 m/s. Nevertheless, we can draw a conclusion that the LSTM is capable of predicting the dynamic response of the nonlinear structure under both small and strong wind inducements. In summary, the surrogate model developed by CNN is not as suitable as the LSTM to predict the dynamic response of the nonlinear structure.

5.3.3 Extreme value prediction of nonlinear transmission tower-line system wind response

To evaluate the LSTM performance on the extreme state of the nonlinear system, the maximum displacement from the dynamic response of each sample is extracted and predicted. Similarly, a comparison analysis with CNN is implemented as well. The differences between the true value and the predicted value for each sample from the testing dataset (20 m/s and 60 m/s) are enumerated in Fig. 18, which shows that the LSTM has lower errors in most samples than the CNN. It is consistent with the RMSEs of the complete sequence predicted by the LSTM (Fig. 16) and provides another evidence that the LSTM is more capable of predicting the maximum displacement of the nonlinear system than CNN.

6. Conclusions

The dynamic response induced by a severe windstorm may result in structural failure and cause other disasters (i.e., power outage after the hurricane). Thus, an efficient and accurate model for dynamic response prediction is urgent for infrastructure safety. This research proposes an advanced method that adopts long short-term memory (LSTM) to predict the structure dynamic response and apply it in the transmission tower-line system. Firstly, the numerical models of transmission tower/tower-line system were designed and simulated by LS-DYNA. Based on the detailed discussion of the LSTM structure, the optimization of LSTM architecture was implemented from the aspects of LSTM layers and hidden units. Meanwhile, the impact of different scales of training dataset on prediction performance was analyzed as well. After that, this research applied the optimized LSTM in the linear system (transmission tower) and the nonlinear system (transmission

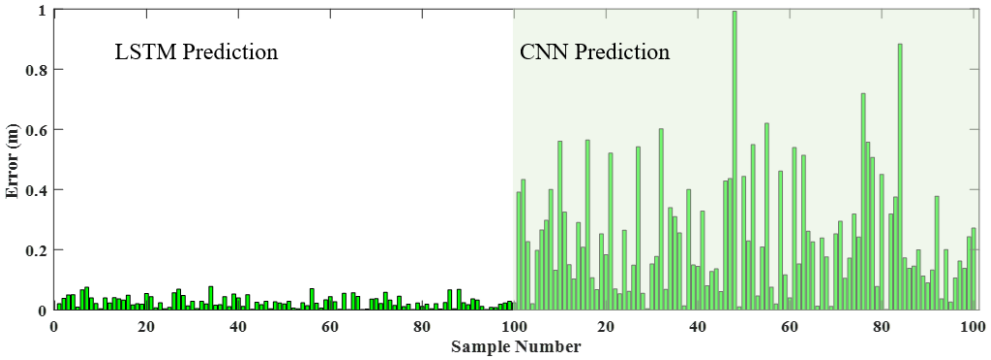

(a) Extreme value prediction when wind speed is 20 m/s

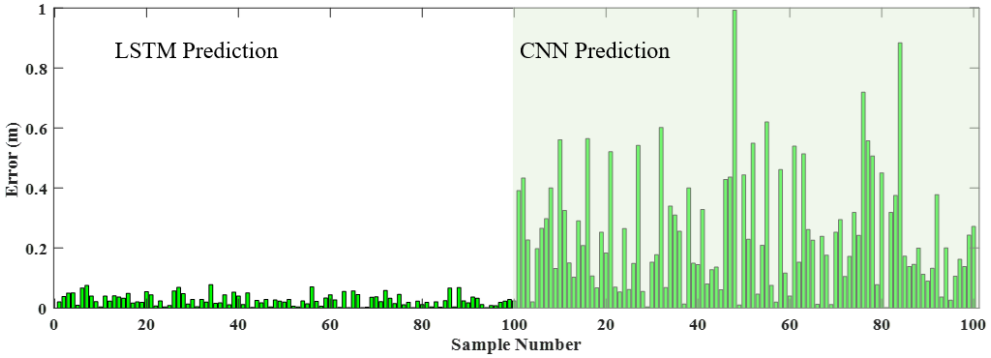

(b) Extreme value prediction when wind speed is 60 m/s

Fig. 18 Error comparison of maximum response (Nonlinear system)

tower-line) with the optimized training dataset to predict the complete sequence of dynamic response and the maximum response. The convolutional neural network (CNN) was selected as the compared method. According to the previous discussion, five lessons have been learned and summarized as follows:

- The architectures of LSTM have a significant influence on the prediction performance. The architecture with 3 LSTM layers and 200 hidden units can achieve the best prediction results in the selected cases of this research.
- There is a trade-off between the prediction accuracy and the computational cost when selecting the training dataset. The larger training dataset can have better prediction accuracy with longer computational cost, and vice versa. According to the discussion, the training dataset with 400 samples is an equilibrium that can have an acceptable prediction RMSEs with low computational time.
- The LSTM can be applied to predict the complete sequence of the dynamic response for both linear system and nonlinear system. The LSTM can capture not only the dynamic trend but also obtain low RMSE, which demonstrates the LSTM capability of dynamic response prediction.
- The maximum response from each sample of both linear system and nonlinear system can be accurately predicted by the LSTM with low RMSE. Since the maximum response normally is the criterion of structural failure under the inducement of severe windstorm, it represents that the LSTM is capable of predicting the extreme state of the linear and nonlinear system.
- Compared with the CNN, the LSTM has comprehensive superiority in predicting the complete sequence of dynamic response and the maximum response for both linear system and nonlinear system with limited data scale.

In conclusion, this research develops a LSTM-based surrogate model that can accurately predict the wind-induced dynamic response and the maximum response for both the linear system and the nonlinear system. This method can be further applied in other infrastructures to predict the wind-induced dynamic response. In the future, the authors will apply this surrogate model in the regional structural response during the wind loads with realistic wind profiles and proper sampling methods.

Acknowledgments

The research work described in this paper was supported by National Science Foundation under award number 1839833 and number 2004658.

References

ASCE 7-98 (1999), Minimum Design Loads for Buildings and Other Structures, American Society of Civil Engineers, Reston, VA, USA.

Cabada, R.Z., Rangel, H.R., Estrada, M.L.B. and Lopez, H.M.C. (2020), "Hyperparameter optimization in CNN for learning-centered emotion recognition for intelligent tutoring systems", *Soft Comput*., **24**(10), 7593-7602. https://doi.org/10.1007/s00500-019-04387-4

Chen, G., Wu, J., Yu, J., Dharani, L.R. and Barker, M. (2001a), "Fatigue assessment of traffic signal mast arms based on field test data under natural wind gusts", *Transport. Res. Record*, **1770**(1), 188-194. https://doi.org/10.3141/1770-24

Chen, F., Li, Q.S., Wu, J.R. and Fu, J.Y. (2011b), "Wind effects on a long-span beam string roof structure: Wind tunnel test, field measurement and numerical analysis", *J. Constr. Steel Res*., **67**(10), 1591-1604. https://doi.org/10.1016/j.jcsr.2011.04.003

Davenport, A.G. (1961), "The spectrum of horizontal gustiness near the ground in high winds", *Quarterly J. Royal Meteorol. Soc*., **87**(372), 194-211. https://doi.org/10.1002/qj.49708737208

Elman, J.L. (1990), "Finding structure in time", *Cognitive Sci*., **14**(2), 179-211. https://doi.org/10.1016/0364-0213(90)90002-E

Fang, C., Tang, H., Li, Y. and Zhang, J. (2020), "Stochastic response of a cable-stayed bridge under non-stationary winds and waves using different surrogate models", *Ocean Eng*., **199**, 106967. https://doi.org/10.1016/j.oceaneng.2020.106967

Fu, X., Li, H.N. and Li, G. (2016), "Fragility analysis and estimation of collapse status for transmission tower subjected to wind and rain loads", *Struct. Safety*, **58**, 1-10. https://doi.org/10.1016/j.strusafe.2015.08.002

Geurts, C., Vrouwenvelder, T., van Staalduinen, P. and Reusink, J. (1998), "Numerical modelling of rain-wind-induced vibration: Erasmus Bridge, Rotterdam", *Struct. Eng. Int*., **8**(2), 129-135. https://doi.org/10.2749/101686698780489351

Ghoshal, A., Sundaresan, M.J., Schulz, M.J. and Pai, P.F. (2000), "Structural health monitoring techniques for wind turbine blades", *J. Wind Eng. Indust. Aerodyn*., **85**(3), 309-324. https://doi.org/10.1016/S0167-6105(99)00132-4

Hamada, A., El Damatty, A.A., Hangan, H. and Shehata, A.Y. (2010), "Finite element modelling of transmission line structures under tornado wind loading", *Wind Struct*., *Int. J*., **13**(5), 451-469. http://dx.doi.org/10.12989/was.2010.13.5.451

He, J., Pan, F., Cai, C.S., Habte, F. and Chowdhury, A. (2018), "Finite-element modeling framework for predicting realistic responses of light-frame low-rise buildings under wind loads", *Eng. Struct*., **164**, 53-69. https://doi.org/10.1016/j.engstruct.2018.01.034

Hochreiter, S. and Schmidhuber, J. (1997), "Long short-term memory", *Neural Computat*., **9**(8), 1735-1780. https://doi.org/10.1162/neco.1997.9.8.1735

Hong, A.L., Ubertini, F. and Betti, R. (2011), "Wind analysis of a suspension bridge: identification and finite-element model simulation", *J. Struct. Eng*., **137**(1), 133-142. https://doi.org/10.1061/(ASCE)ST.1943-541X.0000279

Hopfield, J.J. (1982), "Neural networks and physical systems with emergent collective computational abilities", *Proceedings of the National Academy of Sciences*, **79**(8), 2554-2558. https://doi.org/10.1073/pnas.79.8.2554

Hu, G., Liu, L., Tao, D., Song, J., Tse, K.T. and Kwok, K.C.S. (2020), "Deep learning-based investigation of wind pressures on tall building under interference effects", *J. Wind Eng. Indust. Aerodyn*., **201**, 104138. https://doi.org/10.1016/j.jweia.2020.104138

Hua, X.G., Chen, Z.Q., Lei, X., Wen, Q. and Niu, H.W. (2019), "Monitoring and control of wind-induced vibrations of hanger ropes of a suspension bridge", *Smart Struct. Syst*., *Int. J*., **23**(6), 683-693. https://doi.org/10.12989/sss.2019.23.6.683

Jang, S., Jo, H., Cho, S., Mechitov, K., Rice, J.A., Sim, S.H., Jung, H.J., Yun, C.B., Spencer Jr, B.F. and Agha, G. (2010), "Structural health monitoring of a cable-stayed bridge using smart sensor technology: deployment and evaluation", *Smart Struct. Syst*., *Int. J*., **6**(5_6), 439-459. https://doi.org/10.12989/sss.2010.6.5_6.439

Jordan, M.I. (1986), "Attractor dynamics and parallelism in a connectionist sequential machine", *Proceedings of the Eighth Annual Cognitive Science Society Conference*, Lawrence Erlbaum Associates, August.

Le, V. and Caracoglia, L. (2020), "A neural network surrogate model for the performance assessment of a vertical structure subjected to non-stationary, tornadic wind loads", *Comput. Struct*., **231**, 106208. https://doi.org/10.1016/j.compstruc.2020.106208

Levitan, M.L., Mehta, K.C., Vann, W.P. and Holmes, J.D. (1991), "Field measurements of pressures on the Texas Tech building", *J. Wind Eng. Indust. Aerodyn*., **38**(2-3), 227-234. https://doi.org/10.1016/0167-6105(91)90043-V

Micheli, L., Hong, J., Laflamme, S. and Alipour, A. (2020), "Surrogate models for high performance control systems in wind-excited tall buildings", *Appl. Soft Comput*., **90**, 106133. https://doi.org/10.1016/j.asoc.2020.106133

Mirowski, P. and Vlachos, A. (2015), "Dependency recurrent neural language models for sentence completion", In: *The 53rd Annual Meeting of the Association for Computational Linguistics* (*ACL*), Beijing, China, July.

Molinari, M., Pozzi, M., Zonta, D. and Battisti, L. (2011), "In-field testing of a steel wind turbine tower", *Proceedings of the 28th IMAC*, *A Conference on Structural Dynamics*, New York, USA, June.

Morchid, M. (2018), "Parsimonious memory unit for recurrent neural networks with application to natural language processing", *Neurocomputing*, **314**, 48-64. https://doi.org/10.1016/j.neucom.2018.05.081

National Oceanic and Atmospheric Administration (NOAA) (2018), National hurricane center tropical cyclone report Hurricane Michael, National Hurricane Center, FL, USA. https://www.nhc.noaa.gov/data/tcr/AL142018_Michael.pdf

National Oceanic and Atmospheric Administration (NOAA) (2019), National hurricane center tropical cyclone report Hurricane Dorian, National Hurricane Center, FL, USA. https://www.nhc.noaa.gov/data/tcr/AL052019_Dorian.pdf

Ni, Y.Q., Ko, J.M., Hua, X.G. and Zhou, H.F. (2007), "Variability of measured modal frequencies of a cable-stayed bridge under different wind conditions", *Smart Struct. Syst*., *Int. J*., **3**(3), 341-356. http://dx.doi.org/10.12989/sss.2007.3.3.341

Oh, B.K., Glisic, B., Kim, Y. and Park, H.S. (2019), "Convolutional neural network-based wind-induced response estimation model for tall buildings", *Comput.-Aided Civil Infrastr. Eng*., **34**(10), 843-858. https://doi.org/10.1111/mice.12476

Park, H.S. and Oh, B.K. (2018), "Real-time structural health monitoring of a supertall building under construction based on visual modal identification strategy", *Automat. Constr*., **85**, 273-289. https://doi.org/10.1016/j.autcon.2017.10.025

Park, E.C., Lee, S.H., Min, K.W., Chung, L., Lee, S.K., Cho, S.H., Yu, E. and Kang, K.S. (2008), "Design of an actuator for simulating wind-induced response of a building structure", *Smart Struct. Syst*., *Int. J*., **4**(1), 85-98. http://dx.doi.org/10.12989/sss.2008.4.1.085

Park, J.H., Huynh, T.C., Lee, K.S. and Kim, J.T. (2016), "Wind and traffic-induced variation of dynamic characteristics of a cable-stayed bridge-benchmark study", *Smart Struct. Syst*., *Int. J*., **17**(3), 491-522. http://dx.doi.org/10.12989/sss.2016.17.3.491

Reimers, N. and Gurevych, I. (2017). "Optimal hyperparameters for deep lstm-networks for sequence labeling tasks", In: arXiv preprint, arXiv:1707.06799.

Repetto, M.P. and Solari, G. (2010). "Wind-induced fatigue

collapse of real slender structures", *Eng*. *Struct*., **32**(12), 3888-3898. https://doi.org/10.1016/j.engstruct.2010.09.002

Sun, S.B., He, Y.Y., Zhou, S.D. and Yue, Z.J. (2017), "A data-driven response virtual sensor technique with partial vibration measurements using convolutional neural network", *Sensors*, **17**(12), 2888. http://dx.doi.org/10.3390/s17122888

Tamura, Y., Matsui, M., Pagnini, L.C., Ishibashi, R. and Yoshida, A. (2002), "Measurement of wind-induced response of buildings using RTK-GPS", *J. Wind Eng. Indust. Aerodyn*., **90**(12-15), 1783-1793. https://doi.org/10.1016/S0167-6105(02)00287-8

Tort, C., Şahin, S. and Hasançebi, O. (2017), "Optimum design of steel lattice transmission line towers using simulated annealing and PLS-TOWER", *Comput. Struct*., **179**, 75-94. https://doi.org/10.1016/j.compstruc.2016.10.017

Wong, K.Y., Lau, C.K. and Flint, A.R. (2000), "Planning and implementation of the structural health monitoring system for cable-supported bridges in Hong Kon", In: *Nondestructive evaluation of highways*, *utilities*, *and pipelines IV*. International Society for Optics and Photonics, Newport Beach, CA, USA, March.

Wu, R.T. and Jahanshahi, M.R. (2019), "Deep convolutional neural network for structural dynamic response estimation and system identification", *J. Eng. Mech*., **145**(1), 04018125. https://doi.org/10.1061/(ASCE)EM.1943-7889.0001556

Xue, J., Mohammadi, F., Li, X., Sahraei-Ardakani, M., Ou, G. and Pu, Z. (2020), "Impact of transmission tower-line interaction to the bulk power system during hurricane", *Reliabil. Eng. Syst. Safety*, **203**, 107079. https://doi.org/10.1016/j.ress.2020.107079

Yin, W., Kann, K., Yu, M. and Schütze, H. (2017), "Comparative study of cnn and rnn for natural language processing", arXiv preprint, arXiv:1702.01923.

Zhang, J.W. and Li, Q.S. (2018), "Field measurements of wind pressures on a 600 m high skyscraper during a landfall typhoon and comparison with wind tunnel test", *J. Wind Eng. Indust. Aerodyn*., **175**, 391-407. https://doi.org/10.1016/j.jweia.2018.02.012

Zhang, R., Chen, Z., Chen, S., Zheng, J., Büyüköztürk, O. and Sun, H. (2019), "Deep long short-term memory networks for nonlinear structural seismic response prediction", *Comput. Struct*., **220**, 55-68. https://doi.org/10.1016/j.compstruc.2019.05.006

Zhou, S. and Song, W. (2020), "Deep learning-based roadway crack classification using laser-scanned range images: A comparative study on hyperparameter selection", *Automat. Constr*., **114**, 103171. https://doi.org/10.1016/j.autcon.2020.103171

Zhu, L.D., Li, L., Xu, Y.L. and Zhu, Q. (2012), "Wind tunnel investigations of aerodynamic coefficients of road vehicles on bridge deck", *J. Fluids Struct*., **30**, 35-50. https://doi.org/10.1016/j.jfluidstructs.2011.09.002